Prognosis of Internal Short Circuit Formation in Lithium-Ion Batteries: An Integrated Approach Using Extended Kalman Filter and Regression Model

Lorenzo Brancato[1], Yiqi Jia[2], Marco Giglio[3], and Francesco Cadini[4]

[1] *Politecnico di Milano, Department of Mechanical Engineering, Via La Masa 1, 20156, Milan, Italy*
lorenzo.brancato@polimi.it
yiqi.jia@polimi.it
marco.giglio@polimi.it
**Corresponding author: francesco.cadini@polimi.it*

ABSTRACT

The global transition to electric power, aimed at mitigating climate change and addressing fuel shortages, has led to a rising usage of lithium-ion batteries (LIBs) in different fields, notably transportation. Despite their many benefits, LIBs pose a critical safety concern due to the potential for thermal runaway (TR), often triggered by spontaneous internal short circuit (ISC) formation. While extensive research on LIB fault diagnosis and prognosis exists, forecasting ISC formation in batteries remains unexplored. This paper presents a new methodology that combines the extended Kalman filter (EKF) algorithm for real-time estimation of ISC state with an adaptive linear regressor model for forecasting remaining useful life (RUL). This approach is designed for seamless integration into actual battery management systems, offering a computationally efficient solution. Numerical validation of the framework was conducted due to the current lack of experimental data in the literature. The significance of this work lies in its contribution to ISC prognosis, providing a practical solution to enhance battery safety.

1. INTRODUCTION

In response to the increasing environmental consciousness and the urgent need to address climate change, car manufacturers and consumers are turning towards cleaner alternatives to traditional gasoline-powered vehicles. Electric vehicles (EVs) are at the forefront of this shift, offering significant reductions in emissions that lead to cleaner air and a more sustainable planet. This movement is not just a trend; governments worldwide are actively supporting and encouraging the adoption of EVs through various policies. These include the implementation of stricter emissions regulations, mandates for zero-emission vehicles, and substantial investments in charging infrastructure.

LIBs have emerged as the go-to choice power source in EVs due to their numerous advantages, such as high energy density, powerful performance, and extended lifespan (Ding, Cano, Yu, Lu, & Chen, 2019). Despite their many benefits, LIBs are subjected to degradation phenomena (Han et al., 2019). This continuous degradation poses risks like battery failures and safety hazards, above all TR accidents (Feng, Ouyang, et al., 2018). The most common cause of TR incidents is ISC, making it imperative for the battery management system (BMS) to detect ISC formation and prevent severe ISC formation early. This is pivotal for ensuring the safe and reliable operation of EVs.

Understanding the intricate mechanism behind spontaneous ISC formation is an ongoing area of study that demands further research (Feng, Ouyang, et al., 2018). However, observations indicate that ISC formation, when not triggered by external factors like crushing or penetration, generally progresses slowly (Zhang et al., 2021). Moreover, research has shown that ISC formation predominantly impacts the electrical and thermal properties of the cell (Huang et al., 2021). This suggests that monitoring both the voltage and temperature of the cell, which are typically available in commercial BMS, could be exploited to detect and track ISC formation.

In recent years, researchers have made significant strides in developing various diagnostic algorithms aimed at detecting ISC and preventing TR. Most of these approaches are purely data-driven and aim at identifying parameter inconsistencies among single or multiple cells. These approaches utilize factors such as voltage (Hermann & Kohn, 2013), temperature (Yang, Cui, & Wang, 2019), State of Charge (SoC) (Zheng et al., 2018), and capacity (Reichl & Hrzina, 2018). However,

the subtle changes in electro-thermal signals caused by spontaneous ISC formation may not be immediately discernible within the battery dynamic responses, especially during the early stages of ISC. Additionally, signal variations due to external factors could potentially trigger false alarms. Consequently, establishing a precise threshold value presents a considerable challenge, as this value greatly affects the speed and accuracy of detection.

More advanced data-driven approaches have emerged to address these challenges, harnessing the capabilities of machine learning techniques. These approaches employ models such as deep neural networks (Cui et al., 2024) or random forest (Liu, Hao, Han, Zhou, & Li, 2023). However, since these methods rely solely on existing data, their performance is significantly limited by the scarcity of available data and the difficulties in generating new datasets.

To overcome these limitations, also model-based approaches have been developed to detect ISC. These include equivalent circuit models (ECM) (Asakura, Nakashima, Nakatsuji, & Fujikawa, 2010; Yokotani, 2014; Ikeuchi, Majima, Nakano, & KASA, 2014; Feng, Pan, He, Wang, & Ouyang, 2018), or more advanced electro-chemical models (Ma, Deng, & Wang, 2023). The basic idea of these methods is to transform the problem of ISC detection into model parameters and state estimation. The battery models are established to predict the voltage and temperature of the cells. The measured voltage or temperature of each cell is then compared with the predicted value of the model. If the residual between the two exceeds the allowable error range, it is considered that an ISC has occurred.

This work fills a crucial gap in the literature by focusing on prognosis and predicting the behavior of batteries experiencing spontaneous ISC formation. While there are existing ISC detection methods, as far as the authors are aware, no other studies have delved into predicting the evolution of ISC. What sets apart the prognostic framework introduced in this work is its dual capability: not only does it detect ISC for early warnings, but it also quantifies its severity and forecasts its future progression, enabling timely preventive measures. Moreover, the methodology emphasizes efficiency in selecting models and algorithms, considering their practical implementation in a BMS.

We build the prognostic framework upon the capabilities of the online ISC estimation algorithm proposed by the same authors in Ref. (Jia, Brancato, Giglio, & Cadini, 2024), which, unlike other ISC detection methods:

- utilizes both electrical and thermal measurements to enhance ISC detection and estimation accuracy;
- detect ISC by estimating a model parameter strictly related to the spontaneous ISC formation, allowing also to track the ISC state evolution.

This study introduces a method for predicting the battery RUL probability density function (pdf) using an adaptive linear regressor model to forecast the evolution of the ISC state until an appropriate threshold is reached. The proposed method is designed to be fully automated and can be easily integrated into a BMS for diagnosing and prognosis of spontaneous ISC formation. Moreover, the flexibility of the framework lies in its capacity to accommodate, in principle, various ISC state trajectories.

To validate our approach, we conducted a numerical case study that simulated the effects observed in measurements due to spontaneous ISC formation. This study aims to evaluate the effectiveness of our framework, given the scarcity of experimental data. Gathering such data proves challenging due to the complex nature and associated risks inherent in this phenomenon.

The paper is structured as follows: Section 2 briefly details the methods employed in developing the diagnosis and prognosis framework. In Section 3, the capabilities of the proposed method are demonstrated through a numerical case study involving a cylindrical LIB cell experiencing spontaneous ISC formation. Finally, Section 4 presents the conclusions drawn from this work and suggests potential directions for further research.

2. METHODOLOGY

2.1. Online ISC estimation algorithm

A dynamical system state comprises variables describing its condition and behavior. Non-linear dynamical systems exhibit dynamics not expressible linearly. State-space models represent system dynamics and observations using a hidden state vector $\mathbf{x}$. State equation $\mathbf{f}$ governs state vector evolution with some input $\mathbf{u}$ and some process noise $\mathbf{w}$, while observation equation $\mathbf{h}$ relates observed data, denoted with $\mathbf{y}$, to the state vector $\mathbf{x}$, some input $\mathbf{u}$ and some measurement noise $\mathbf{n}$.

The EKF estimates non-linear system states (Simon, 2006). It approximates non-linear dynamics linearly via Taylor expansion. The algorithm involves two steps: prediction, estimating the next state ($\hat{\mathbf{x}}$) and observations ($\hat{\mathbf{y}}$) with the previous state and calculating error covariance matrix ($\Sigma_{\hat{\mathbf{x}}}$); correction, updating state estimate and covariance with weighted innovation terms based on system observations. Proper initialization of the algorithm is crucial, assigning values to state vector estimate and error covariance matrix. The full algorithm is detailed in Table 1.

The electro-thermal model of a cylindrical cell described in our previous work (Jia et al., 2024), whose governing equations and parameters are summarized in Table 2 and Table 3, is discretized in time considering the following augmented state vector that includes the equivalent ISC conductance parameter G_{ISC}, expressed in Ω^{-1}, and representative of the

Table 1. Description of the extended Kalman filter algorithm.

Extended Kalman Filter Algorithm
Initialization:
Initialize state estimate $\hat{\mathbf{x}}_0^-$ and error matrix covariance $\Sigma_{\hat{\mathbf{x}}_0^-}$
Prediction Step:
Predict the state estimate:
$\hat{\mathbf{x}}_k^- = \mathbf{f}(\hat{\mathbf{x}}_{k-1}^+, \mathbf{u}_{k-1}, \bar{\mathbf{w}}_{k-1})$
Predict the observations:
$\hat{\mathbf{y}}_k = \mathbf{h}(\hat{\mathbf{x}}_{k-1}^+, \hat{\mathbf{y}}_{k-1}, \mathbf{u}_{k-1}, \bar{\mathbf{n}}_{k-1})$
Predict the error covariance matrix:
$\Sigma_{\hat{\mathbf{x}}_k^-} = A_k \Sigma_{\hat{\mathbf{x}}_{k-1}^-} A_k^T + B_k \Sigma_{\mathbf{w}} B_k^T$
Correction Step:
Compute the Kalman gain matrix:
$K_k = \Sigma_{\hat{\mathbf{x}}_k^-} C_k^T (C_k \Sigma_{\hat{\mathbf{x}}_k^-} C_k^T + D_k \Sigma_{\mathbf{n}} D_k^T)^{-1}$
Update the state estimate:
$\hat{\mathbf{x}}_k^+ = \hat{\mathbf{x}}_k^- + K_k(\mathbf{y}_k - \hat{\mathbf{y}}_k)$
Update the error covariance matrix:
$\Sigma_{\hat{\mathbf{x}}_k^+} = \Sigma_{\hat{\mathbf{x}}_k^-} - K_k(C_k \Sigma_{\hat{\mathbf{x}}_{k-1}^-} C_k^T + D_k \Sigma_{\mathbf{n}} D_k^T) K_k^T$
Where:
$A_k = \frac{\partial \mathbf{f}}{\partial \mathbf{x}}\big\|_{\hat{\mathbf{x}}_{k-1}^+, \mathbf{u}_{k-1}, \bar{\mathbf{w}}_{k-1}}$ $B_k = \frac{\partial \mathbf{f}}{\partial \mathbf{w}}\big\|_{\hat{\mathbf{x}}_{k-1}^+, \mathbf{u}_{k-1}, \bar{\mathbf{w}}_{k-1}}$
$C_k = \frac{\partial \mathbf{h}}{\partial \mathbf{x}}\big\|_{\hat{\mathbf{x}}_{k-1}^+, \mathbf{u}_{k-1}, \bar{\mathbf{n}}_{k-1}}$ $D_k = \frac{\partial \mathbf{h}}{\partial \mathbf{n}}\big\|_{\hat{\mathbf{x}}_{k-1}^+, \mathbf{u}_{k-1}, \bar{\mathbf{n}}_{k-1}}$
and $\Sigma_{\mathbf{w}}$, $\Sigma_{\mathbf{n}}$ are the covariance matrices of the two independent, zero-mean, Gaussian processes **w** and **n**.

actual ISC state:

$$\mathbf{x} = [z,\ i_{RC_1},\ i_{RC_2}, h,\ G_{ISC},\ T]^T \tag{9}$$

where z is the dimensionless state-of-charge (SoC), i_{RC_1} and i_{RC_2} are the two polarization currents (expressed in A), and T is the surface temperature (expressed in K).

Finally, the input vector and the output vector are defined as follow:

$$\mathbf{u} = [i_t,\ v_t]^T \tag{10}$$

$$\mathbf{y} = [v_t,\ T]^T \tag{11}$$

assuming that the load current i_t, the terminal voltage v_t, and the surface temperature T are all measurable quantities.

2.2. RUL estimation via simple linear regression

A simple linear regression model describes the linear relationship between a dependent variable, y, also known as the response, and one independent variable, x, also known as the predictor. In general, a simple linear regression model can be a model of the form:

$$y_i = \beta_0 + \beta_1 x_i + \varepsilon_i,\ \ i = 1, ..., n \tag{12}$$

where n is the number of observations, y_i is the i-th response, β_0 is the model constant, β_1 is the slope of the model, ε_i is the i-th error term that captures the variability in y_i that is not explained by the linear relationship with x_i (Seber & Lee, 2012). The usual assumptions for simple linear regression modeling are: (i) the error terms ε_i are uncorrelated; (ii) the error terms ε_i have independent and identical normal distributions with mean zero and constant variance, σ_ε^2; (iii) the responses y_i are uncorrelated.

In this study, we develop an approach to predicting the evolution of ISC state using a simple linear regression model. Here, the response variable is the estimated equivalent ISC resistance, denoted as R_{ISC}, which can be calculated as $1/G_{ISC}$. This estimate is obtained from the equivalent ISC conductance while cycling the battery cell. The predictor variable in our model is the number of cycles, denoted as N. To ensure adaptability, our approach involves fitting the simple linear regression model using a robust least squares estimation algorithm (Holland & Welsch, 1977) within a sliding window of fixed size W. This means that although the number of observations analyzed remains constant at $n = W$, the actual data points y_i can vary between each query. To address the uncertainties in our predictions, once the model is fit with the latest available data points, we generate different realizations of the ISC evolution by sampling from the estimated Gaussian distribution of the error terms, $\varepsilon_i \sim N(0, \sigma_\varepsilon)$. These realizations are then truncated when they reach a predetermined threshold for the ISC state value. Through this process, we estimate the pdf of the RUL.

3. RESULTS

In this section, we validate the performance of the framework proposed in this work through a numerical study due to the scarcity of experimental data in existing literature.

3.1. Simulating spontaneous ISC formation

To maintain simplicity and ensure consistency with our methodology, we use the electro-thermal battery model described in Section 2.1 to simulate the dynamics of a real battery cell. In practice, the voltage and surface temperature signals processed by the proposed online ISC estimation algorithm are generated by this same model, hereafter referred to as "the plant". Nonetheless, we equip the plant with appropriate noise generators to capture non-modeled dynamics.

In the plant, it is assumed that the progression of degradation follows a power-law pattern over time:

$$\begin{cases} R_{ISC}(t) = R_i - (R_f - R_i) \cdot \left(\frac{t}{T_{end}}\right)^{p(T)} \\ p(T) = p_0 \cdot e^{-\frac{c}{T}} \end{cases} \tag{13}$$

Table 2. The governing equations of the electro-thermal model.

Equation name	Equation expression	
Current Kirchhoff law	$i = i_t + i_{ISC}$, with $i_{ISC} = v_t / R_{ISC}$	(1)
Voltage Kirchhoff law	$v_t = \text{OCV}(z) + M_0 \text{sign}(i) + Mh - R_1 i_{R_1} - R_2 i_{R_2} - R_0 i$	(2)
Coulomb counting	$\frac{dz}{dt} = -\frac{\eta}{Q} i$	(3)
RC circuit dynamics	$\frac{di_{RC_j}}{dt} = -\frac{1}{R_j C_j} i_{RC_j} - \frac{1}{R_j C_j} i$, with $j = 1, 2$	(4)
Hysteresis dynamics	$\frac{dh}{dt} = -\left\lvert \frac{\gamma\eta}{Q} i \right\rvert h - \left\lvert \frac{\gamma\eta}{Q} i \right\rvert \text{sign}(i)$	(5)
Electrical heat	$Q_{in} = R_0 i^2 + \frac{v_t^2}{R_{ISC}}$	(6)
Dissipated heat	$Q_{out} = h_{conv}(T - T_{amb})A$	(7)
Heat balance	$\frac{dT}{dt} = -\frac{1}{mc_m}(Q_{in} - Q_{out})$	(8)

Where i_t is the load current, v_t is the terminal voltage, z is the state of charge, i_{RC_j} are the polarization currents, h is the unitless hysteresis state, and T is the surface temperature.

Table 3. Model parameters.

Parameter name	Symbol	Value	Unit
Open-circuit voltage	OCV	$f(z)$	V
Series resistance	R_0	9.18	mΩ
1st polarization resistance	R_1	2.53	mΩ
2nd polarization resistance	R_1	21.32	mΩ
1st polarization capacitance	C_1	5116	F
2nd polarization capacitance	C_1	3582	F
Instantaneous hysteresis voltage term	M_0	0	V
Dynamic hysteresis voltage term	M	0.16	V
Coulombic efficiency	η	0.994	–
Rate of decay constant	γ	1	–
Capacity	Q	2.05	Ah
Battery cell mass	m	76	g
Specific heat capacity	c_m	1095	J/KgK
Heat transfer convection coefficient	h_{conv}	10	$\text{W/m}^2\text{K}$
Battery outer surface	A	5.3×10^{-3}	m^2
Ambient temperature	T_{amb}	298	K

Here the exponent p is a variable that changes with temperature, behaving according to an Arrhenius function; R_i is the initial ISC resistance value; R_f is the final ISC resistance value; T_{end} is the cycling time needed to evolve from R_i to R_f; p_0 and c are respectively the Arrhenius constant and rate terms. The values of these parameters are indicated in Table 4

Table 4. Degradation model parameters.

Parameter name	Symbol	Value	Unit
Initial ISC resistance value	R_i	1000	Ω
Final ISC resistance value	R_f	0.1	Ω
Cycling time from R_i to R_f	T_{end}	1200	h
Arrhenius constant term	p_0	3278	–
Arrhenius rate term	c	3.1×10^{-3}	K

The degradation model, which also incorporates a temperature-dependent exponent, is formulated and parameterized based on the following assumptions:

- ISC persists throughout the entire lifespan of the cell, with its formation and evolution spanning hundreds of hours or more (Zhang et al., 2021);
- As ISC progresses, the internal temperature of the cell increases, leading to complex chemical reactions involving electrode materials, electrolyte, and separator (Feng, Ouyang, et al., 2018);
- Most of these chemical reactions are exothermic, accelerating the TR occurrence. When the temperature overcomes a critical point, various degradation phenomena occur, such as solid-electrolyte interphase layer decomposition, anode-electrolyte reactions, electrolyte breakdown, separator meltdown, and cathode failure. All these phenomena contribute to further increasing the internal temperature of the cell, ultimately triggering TR (Feng, Ouyang, et al., 2018).

The way the degradation sub-model described by Eq. (13) relates to the electro-thermal cell model summarized by the equations in Table 2 is graphically illustrated in Figure 1. This model is simulated by cycling the plant using a dynamic stress test current cycle and constant charging. The resulting ISC state evolution is illustrated at the top of Figure 2, where the

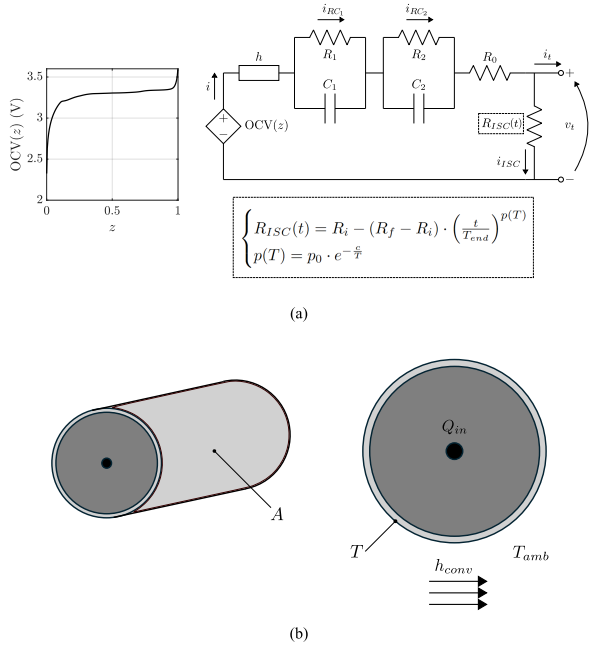

Figure 1. Electro-thermal battery cell model subjected to spontaneous ISC degradation model evolution. (a) Electrical sub-model coupled with the ISC degradation model. (b) Thermal sub-model.

x-axis has been scaled to cycles and the y-axis has been log-scaled to enhance visibility.

During the simulation, some important health-related quantities, i.e., the maximum temperature, T_{max}, and the discharging time, t_{dis}, measured across one cycle, have also been recorded along with the voltage and temperature measurements. These quantities are shown at the bottom of Figure 2. These quantities are, in fact, strongly correlated with the severity of the ISC. The observed trends agree with those expected for spontaneous ISC formation, as referenced in (Feng, Pan, et al., 2018). Figure 2 further outlines three distinct regions with dotted lines that correspond to the ISC severity state in the plant. These states are defined based on the observed effects on the aforementioned health-related quantities: in the soft ISC region, these quantities exhibit minimal changes; in the moderate ISC region, these changes become more noticeable; in the severe ISC region, the changes are extremely significant.

3.2. Prognosis

To save memory space and computational costs, we only store the data points of the Gaussian posterior pdf estimate of the ISC state obtained from the EKF at the end of each cycle. This decision is made considering that the ISC state is not expected to change significantly within a single working cycle. Although the online ISC estimation algorithm is designed to acquire and store data every second, we prioritize saving only

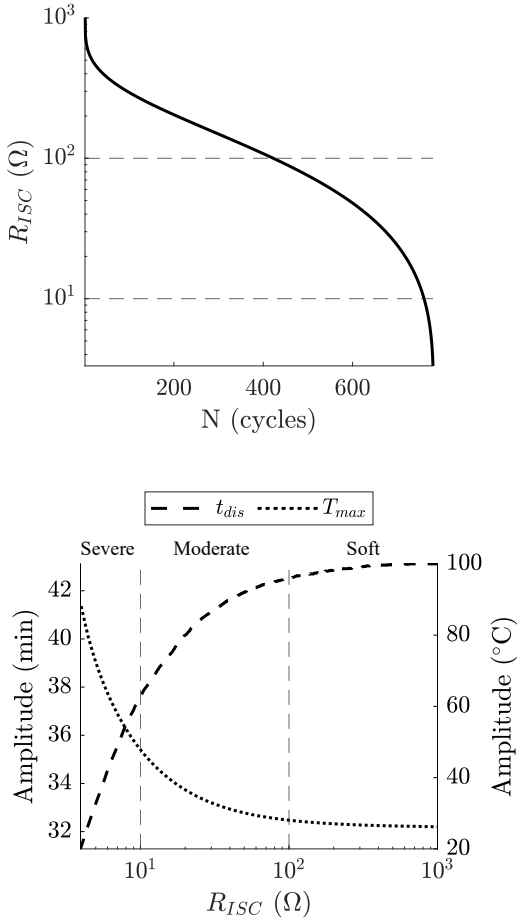

Figure 2. Top: ISC state evolution in the plant during cycling. Bottom: evolution of the maximum temperature T_{max} and the discharging time t_{dis} measured across one cycle.

these specific data points to local memory.

When enough data is available in the local memory, the user can request the prognosis. In this study, we define the prognosis triggering point as when the estimated ISC state enters the moderate ISC region, specifically when $\hat{R}_{ISC} \leq 100\Omega$, as indicated at the top of Figure 3. Additionally, we use a sliding window size W of 50 data points to ensure the linear regressor model captures the local trend behavior. This can be seen in the bottom part of Figure 3, which illustrates the linear regression at the prognosis query $N = 520$ cycles.

After fitting the parameters of the linear regressor model, the RUL pdf is computed. This is done by moving forward in time with the fitted model, sampling different realizations of the error terms from the estimated Gaussian distribution,

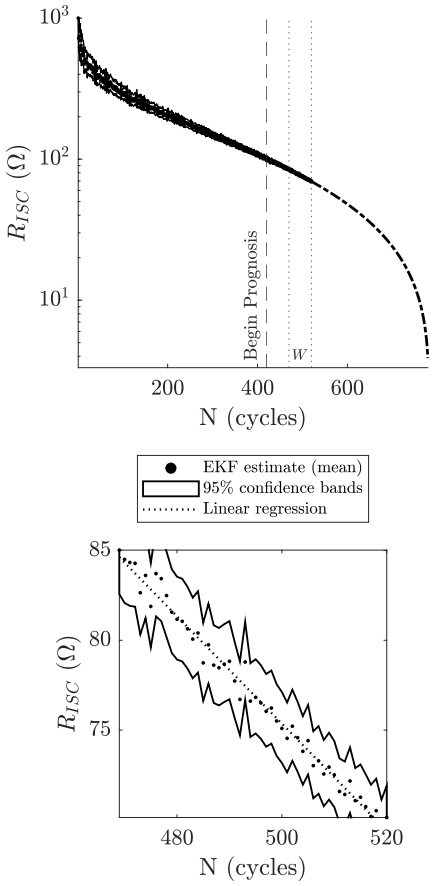

Figure 3. Top: Example of prognosis query when $N = 520$ cycles, outlining the sliding window W. Bottom: Linear regression on the latest available data points in the sliding window.

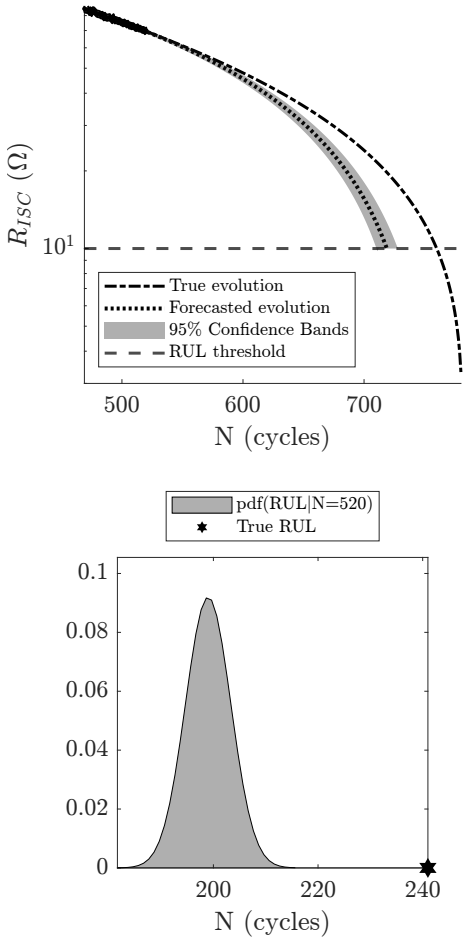

Figure 4. Top: predicted ISC state trajectory when $N = 520$ cycles. Bottom: corresponding RUL pdf estimation.

$\varepsilon_i \sim N(0, \sigma_\varepsilon)$, to account for modeling uncertainties. The prediction is then truncated up to a threshold value of 10 Ω to prevent the system from entering the severe ISC region. This process, at the prognosis query $N = 520$ cycles, is illustrated in Figure 4.

By repeating this process at different prognosis queries the RUL pdf prediction evolution is obtained, as shown in Figure 5, and compared with the actual RUL evolution of the plant. The results demonstrate the satisfactory performances obtained with the proposed method. The estimated RUL steadily converges to the true RUL value. However, the results consistently suggest that the true RUL is far outside the 95% confidence interval. This is because the linear regressor model can well approximate the local degradation behavior with good accuracy. However, the latter changes as ISC progresses due to the aforementioned exothermic electrochemical reactions, which are accounted for with the degradation model described in Eq. (13) considering an Arrhenius-like term. Furthermore, the confidence bounds narrow progressively as the prognosis steps advance, due to the increased accuracy of the EKF estimation as the ISC state becomes more severe, as also can be appreciated on top of Figure 3. This, in turn, leads to a smaller variance of the residuals with the estimated linear regressor at a later prognosis query, when the ISC state is more severe.

4. CONCLUSION

This work presents a prognosis framework for spontaneous ISC formation. The proposed framework leverages the potentialities of an EKF algorithm to online estimate and track the evolution of the equivalent ISC resistance value, which is a quantity representative of the actual ISC state of the battery cell. At appropriate instants, some of the estimated ISC resistance values are saved to local memory. The stored data are then processed for prognosis. When enough data are stored,

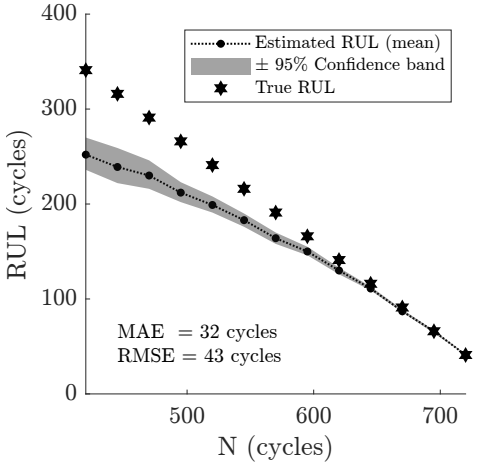

Figure 5. Comparison between true RUL evolution and predicted RUL evolution.

the user can request the prognosis algorithm to predict the battery RUL pdf. This is done by employing a linear regressor model for the prediction and a Monte Carlo simulation for quantifying the uncertainties involved. This work establishes a first step toward effective spontaneous ISC formation prognosis. Due to the lack of experimental data in the literature, the proposed approach has been validated numerically with synthetic measurements that aim to accurately reproduce the expected effects ISC has on the electrical and thermal characteristics of the cell. Furthermore, a degradation model that reasonably reproduces the expected evolution of ISC has been constructed based on certain assumptions that may not be fulfilled with real experimental data. Nevertheless, the framework proposed could in principle accommodate different degradation trajectories. Consequently, to further validate the approach, future studies will apply the methodology to real experimental data on spontaneous ISC formation as soon as the latter is available. On top of that, the method could be improved by using more sophisticated regressor models, such as ARIMA or NARX models, to improve the RUL prediction performance for a cell subjected to spontaneous ISC formation.

REFERENCES

Asakura, J., Nakashima, T., Nakatsuji, T., & Fujikawa, M. (2010, July 29). *Battery internal short-circuit detecting device and method, battery pack, and electronic device system.* Google Patents. (US Patent App. 12/670,597)

Cui, B., Wang, H., Li, R., Xiang, L., Zhao, H., Xiao, R., … others (2024). Ultra-early prediction of lithium-ion battery performance using mechanism and data-driven fusion model. *Applied Energy*, *353*, 122080.

Ding, Y., Cano, Z. P., Yu, A., Lu, J., & Chen, Z. (2019). Automotive li-ion batteries: current status and future perspectives. *Electrochemical Energy Reviews*, *2*, 1–28.

Feng, X., Ouyang, M., Liu, X., Lu, L., Xia, Y., & He, X. (2018). Thermal runaway mechanism of lithium ion battery for electric vehicles: A review. *Energy storage materials*, *10*, 246–267.

Feng, X., Pan, Y., He, X., Wang, L., & Ouyang, M. (2018). Detecting the internal short circuit in large-format lithium-ion battery using model-based fault-diagnosis algorithm. *Journal of Energy Storage*, *18*, 26–39.

Han, X., Lu, L., Zheng, Y., Feng, X., Li, Z., Li, J., & Ouyang, M. (2019). A review on the key issues of the lithium ion battery degradation among the whole life cycle. *ETransportation*, *1*, 100005.

Hermann, W. A., & Kohn, S. I. (2013, December 31). *Detection of over-current shorts in a battery pack using pattern recognition.* Google Patents. (US Patent 8,618,775)

Holland, P. W., & Welsch, R. E. (1977). Robust regression using iteratively reweighted least-squares. *Communications in Statistics - Theory and Methods*, *6*(9), 813-827.

Huang, L., Liu, L., Lu, L., Feng, X., Han, X., Li, W., … others (2021). A review of the internal short circuit mechanism in lithium-ion batteries: Inducement, detection and prevention. *International Journal of Energy Research*, *45*(11), 15797–15831.

Ikeuchi, A., Majima, Y., Nakano, I., & KASA, K. (2014, July 3). *Circuit and method for determining internal short-circuit, battery pack, and portable device.* Google Patents. (US Patent App. 14/196,101)

Jia, Y., Brancato, L., Giglio, M., & Cadini, F. (2024). Temperature enhanced early detection of internal short circuits in lithium-ion batteries using an extended kalman filter. *Journal of Power Sources*, *591*, 233874.

Liu, H., Hao, S., Han, T., Zhou, F., & Li, G. (2023). Random forest-based online detection and location of internal short circuits in lithium battery energy storage systems with limited number of sensors. *IEEE Transactions on Instrumentation and Measurement*.

Ma, R., Deng, Y., & Wang, X. (2023). Simplified electrochemical model assisted detection of the early-stage internal short circuit through battery aging. *Journal of Energy Storage*, *66*, 107478.

Reichl, T., & Hrzina, P. (2018). Capacity detection of internal short circuit. *Journal of Energy Storage*, *15*, 345–349.

Seber, G. A., & Lee, A. J. (2012). *Linear regression analysis*. John Wiley & Sons.

Simon, D. (2006). *Optimal state estimation: Kalman, h infinity, and nonlinear approaches*. John Wiley & Sons.

Yang, B., Cui, N., & Wang, M. (2019). Internal short circuit fault diagnosis for lithiumion battery based on voltage and temperature. In *2019 3rd conference on vehicle control and intelligence (cvci)* (pp. 1–6).

Yokotani, K. (2014, February 4). *Battery system and method for detecting internal short circuit in battery system.* Google Patents. (US Patent 8,643,332)

Zhang, G., Wei, X., Tang, X., Zhu, J., Chen, S., & Dai, H. (2021). Internal short circuit mechanisms, experimental approaches and detection methods of lithium-ion batteries for electric vehicles: A review. *Renewable and Sustainable Energy Reviews*, *141*, 110790.

Zheng, Y., Gao, W., Ouyang, M., Lu, L., Zhou, L., & Han, X. (2018). State-of-charge inconsistency estimation of lithium-ion battery pack using mean-difference model and extended kalman filter. *Journal of Power Sources*, *383*, 50–58.

BIOGRAPHIES

Lorenzo. BRANCATO was born in Italy on December 12, 1998. He earned his Bachelor's degree in Mechanical Engineering from Politecnico di Milano in 2020. Subsequently, he pursued a Master's degree in Mechatronic Engineering at Politecnico di Milano, completing his studies in 2022. He has started his Ph.D in Mechanical Engineering at Politecnico di Milano in 2023. His current research focus on the development of advanced diagnostic and prognostic approaches for dynamic, complex systems subject to degradation. This involves high-fidelity multi-physics modeling, simulation and model-based filtering methods.

Yiqi. JIA was born in China on January 28, 1996. She holds a Bachelor's degree in Automotive Engineering from Wuhan University of Technology, Wuhan, China (2017), and a Master's degree in Automotive Engineering from the University of Bath, Bath, UK (2018). After working as a vehicle engineer for nearly 3 years at Ford Motor Company, she started her Ph.D. journey in Mechanical Engineering at Politecnico di Milano in November 2021. Her research primarily focuses on the diagnosis and prognosis of Lithium-ion batteries, structural batteries, and more broadly, on mechanical/structural-related behaviors. This includes battery modeling, simulation, and data-based estimation methods for optimal battery management.

Marco. GIGLIO is Full Professor at the Department of Mechanical Engineering, Politecnico di Milano. His main research fields are: (i) Structural integrity evaluation of complex platforms through Structural Health Monitoring methodologies; (ii) Vulnerability assessment of ballistic impact damage on components and structures, in mechanical and aeronautical fields; (iii) Calibration of constitutive laws for metallic materials; (iv) Expected fatigue life and crack propagation behavior on aircraft structures and components; (v) Fatigue design with defects. He has been the coordinator of several European projects: HECTOR, Helicopter Fuselage Crack Monitoring and prognosis through on-board sensor, 2009-2011; ASTYANAX (Aircraft fuselage crack Monitoring System and Prognosis through eXpert onboard sensor networks), 2012-2015; SAMAS (SHM application to Remotely Piloted Aircraft Systems), 2018-2020. He has been the project leader of the Italian Ministry of Defence project in the National Plan of Military Research, SUMO (Development of a predictive model for the ballistic impact), 2011-2012, and SUMO 2 (Development of an analytical, numerical and experimental methodology for the design of ballistic multilayer protections), 2017-2019. He has published more than 210 papers, h-index 27 (source Scopus) in referred international journals and congresses.

Francesco. CADINI (MSc in Nuclear Engineering, Politecnico di Milano, 2000; MSc in Aerospace Engineering, UCLA, 2003; PhD in Nuclear Engineering, Politecnico di Milano, 2006) is Associate Professor at the Department of Mechanical Engineering, Politecnico di Milano. He has more than 20 years of experience in the assessment of the safety and integrity of complex engineering systems, entailing (i) artificial intelligence (machine learning)-based approaches for classification and regression, (ii) development and application of advanced Monte Carlo algorithms for reliability analysis (failure probability estimation), (iii) diagnosis and prognosis (HUMS) of dynamic, complex systems subject to degradation, (iv) uncertainty and sensitivity analyses, (v) structural reliability analyses.